Resonant and Off-Resonant Light-Driven Plasmons in Metal Nanoparticles Studied by Femtosecond-Resolution Third-Harmonic Generation

B. Lamprecht, J. R. Krenn, A. Leitner, and F. R. Aussenegg
Institut für Experimentalphysik, Karl-Franzens Universität Graz, Universitätsplatz 5, A-8010 Graz, Austria
(Received 8 June 1999)

We report on a femtosecond-resolution study of the plasmon fields in gold nanoparticles using third-harmonic generation. Controlled resonant and off-resonant plasmon excitation is achieved by tailoring the nanoparticle sample by an electron-beam-lithographic method. Comparing the measured third order interferometric autocorrelation function of the plasmon field with simulations based on a simple harmonic oscillator model we extract the temporal characteristic of the plasmon oscillation. For off-resonant excitation of particle plasmons we find a beating between the driving laser field and the plasmon field which demonstrates clearly the nature of the plasmon as a collective electron oscillation.

PACS numbers: 78.47.+p, 61.46.+w, 73.20.Mf

In metal nanoparticles resonant collective oscillations of the conduction electrons (particle plasmons) can be excited by light in the visible spectral range. The resonance frequency of a particle plasmon is determined mainly by the dielectric functions of the metal and the surrounding medium, respectively, and by the particle shape, i.e., the ratio of the particle principal axes. Resonance leads to a narrow spectrally selective absorption and an enhancement of the local light field confined on and close to the surface of the metal particle [1]. The spectral width of absorption and near-field enhancement is given by the decay time of the particle plasmons. This decay time is determined by various damping mechanisms acting on the oscillating electrons, as the electronic conductivity of the metal at light frequencies and radiation damping in the case of particle diameters exceeding the Rayleigh limit.

Particle plasmons have been a subject of extensive experimental and theoretical work, resulting in a quite comprehensive understanding of the steady state properties of this phenomenon. Recently also the dynamic aspects of particle plasmons have been addressed by fs time-resolved measurements based on second harmonic generation (SHG) [2–5]. As SHG enhancement originates from the enhanced near field of the plasmon oscillation, SHG can be considered a suitable noninvasive probe of plasmon dynamics. The experiments revealed that the decay of particle plasmons which can be described as the loss of coherence of the oscillating electrons (dephasing) occurs on a sub-10 fs time scale [5].

In this Letter we report on first fs time-resolved measurements of the particle plasmon dynamics relying on third harmonic generation (THG) as a noninvasive monitor for particle plasmon dynamics. By using THG we eliminate a major drawback of SHG-based methods which are restricted to noncentrosymmetric particle shapes. Furthermore we achieve an unprecedented control of resonant and off-resonant plasmon excitation conditions by tailoring nanoparticle samples by a lithographic method [6]. This enables us to deduce the temporal characteristics and the decay time of particle plasmons for resonant and off-resonant excitation, respectively, and thus to gain deepened insight into the physics of particle plasmons.

To model the time dependent particle plasmon field we apply a damped harmonic oscillator driven by a given force $K(t)$. The harmonic approach is justified as the anharmonicity of the plasmon oscillation producing THG is sufficiently small not to influence the linear temporal behavior of the plasmon oscillation. It follows that the particle plasmon field $E_{\mathrm{Pl}}(t)$ is proportional to [7]

$$E_{\mathrm{Pl}}(t) \propto \int_{-\infty}^{t} \frac{1}{\omega_0} K(t^*) e^{-\gamma(t-t^*)} \sin[\omega_0(t - t^*)]\, dt^* \quad (1)$$

with $\omega_0 = 2\pi c/\lambda_{\mathrm{res}}$ and $\gamma = 1/2\tau$, where λ_{res} denotes the resonance wavelength which corresponds to the resonance frequency ω_0, c is the speed of light, and τ is the oscillator energy decay time. Experimentally we determine the third order interferometric autocorrelation function (ACF) [8,9] of $E_{\mathrm{Pl}}(t)$ by measuring the frequency tripled radiation from the nanoparticles after exciting the plasmon oscillations by two identical femtosecond laser pulses separated by a variable time delay t'. Thus in the calculation $K(t)$ is set proportional to $E_{\mathrm{pulse}}(t) + E_{\mathrm{pulse}}(t + t')$, i.e., the sum of two laser pulse fields $E_{\mathrm{pulse}}(t)$ separated by the time delay t'. The calculation of THG intensities is performed by taking the sixth power of $E_{\mathrm{Pl}}(t)$ and integrating the result in time due to the finite response time of the detector. To obtain the third order ACF we perform this calculation procedure for different t' values covering the whole experimentally relevant time delay scan range. The resulting shape of the envelope of the third order ACF is unambiguously determined by the time characteristic of $E_{\mathrm{Pl}}(t)$. We find this temporal characteristic of the plasmon field by fitting the experimentally determined ACF with calculated ACFs with τ as the only fit parameter.

In the experiment we use a Kerr-lens-mode locked Ti:sapphire laser for excitation, which delivers 15 fs pulses at a fixed center wavelength of 774 nm [10]. For a pulse

repetition rate of 71 MHz we measure a cw power of 20 mW on the sample. The pulses are collinearly focused on the sample with a focus diameter of 90 μm, resulting in an energy fluence of $\sim 4\ \mu\mathrm{J/cm}^2$. The high pulse intensity in combination with a low energy per pulse guarantees satisfactory sensitivity for THG measurements without heating the electron gas or even destroying the sample. The third order ACF is measured with a symmetric collinear interferometric optical autocorrelator [11]. The third harmonic signal at $\lambda = 258$ nm is transmitted to a photomultiplier through an optical bandpass filter which blocks the radiation at the fundamental and the second harmonic wavelengths. To obtain a high signal to noise ratio we use lock-in detection.

Our samples consist of regular two-dimensional arrays of in top view circularly shaped Au nanoparticles on a indium-tin oxide (ITO) coated quartz substrate, produced by an electron-beam-lithographic method [5]. We produced arrays of gold particles with a particle height of 14 nm and a particle diameter ranging from 110 to 180 nm. As the particle shape (ratio of the particle principal axes) determines the spectral position of the plasmon resonance, this results in particle plasmon resonance frequencies from 710 to 860 nm. The grating constant of all particle arrays was set to 450 nm. By analysis of scanning electron microscope images the particles within one sample array were found to be nearly monodisperse in shape, in accordance with previous results on similar samples [12].

As mentioned above, the driving laser pulse field has to be known for simulating the THG-ACF. Thus, first of all we have to determine the temporal shape of the laser pulses. For this purpose we measure the third order ACF of the laser pulse itself (see solid line in Fig. 1a) using a 25 μm thick beta borium borate (BBO) crystal as a THG medium with an instantaneous response to the incoming laser pulse field. The temporal shape of the laser pulse is found by fitting the experimentally obtained ACF by a calculated one varying the time function $E_{\mathrm{pulse}}(t)$. The best fit was found by using the Fourier transformed spectrum of the laser pulse for $E_{\mathrm{pulse}}(t)$ (transform limited case); see Figs. 1b and 1c for the laser pulse spectrum and the Fourier transformed spectrum, respectively. The numerical result is compared to the measured ACF of the laser pulse in Fig. 1a, where for the clarity of presentation only the upper envelope of the calculated ACF is marked by the filled circles. We find an excellent agreement with the experimental data.

We now replace the BBO crystal by a nanoparticle array. For *resonant* excitation of nanoparticles (extinction maximum at 774 nm) the resulting third order ACF is shown in Fig. 2a. Because of the finite lifetime of the particle plasmons, a broadening of this ACF in comparison with the ACF of the laser pulse itself is found by comparing Figs. 2a and 1a. The resulting calculated ACF (again only the upper envelope of the calculated ACF is shown by the filled circles for clarity of presentation) shows the

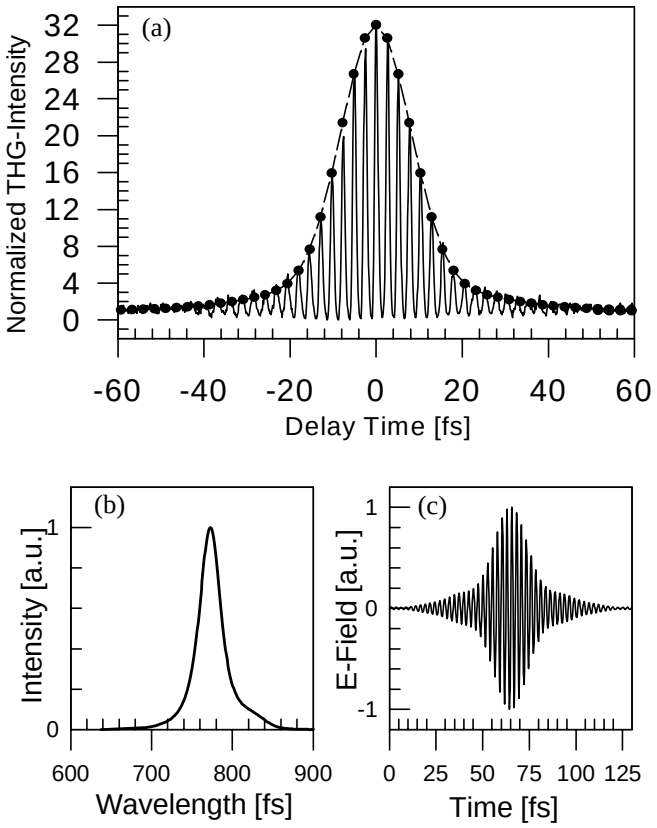

FIG. 1. (a) Solid line: measured third order ACF of the laser pulse (maximum normalized to 32); filled circles: envelope of the calculated ACF (the dashed line serves as a guide to the eye). (b) Spectrum of the fs laser pulse train. (c) Fourier transformed laser pulse spectrum (which is found to be equivalent to the temporal shape of the laser pulse) serves as the driving laser pulse field in the model calculations.

best agreement with the experimental ACF when assuming $\tau = 6$ fs. This value corresponds to the particle plasmon lifetime measured with SHG on similar samples [2]. The deduced temporal evolution of the plasmon field [Eq. (1)] driven by the laser pulse field $E_{\mathrm{pulse}}(t)$ obtained above is shown in Fig. 2b. Furthermore we find the experimental peak to background ratio to be equal to 32:1, the very value predicted by theory. This result confirms that in the case of excitation with fs pulses in the low laser fluence regime there are no changes in the acting THG optical nonlinearity due to electron gas heating during the measurement time [13,14].

The THG-ACF for an *off-resonant* particle plasmon excitation (particle array extinction maximum at 860 nm) is shown in Fig. 3a. We find the full width at half maximum (FWHM) of this ACF to be even smaller than that of the laser pulse itself. Furthermore small side wings near the main peak of the ACF function emerge. Again, assuming $\tau = 6$ fs the numerical simulation yields a third order ACF (envelope shown in Fig. 3a) which agrees well with the measured one. Note that the side wings are well reproduced by the model calculation. The calculated temporal behavior of the plasmon field for the off-resonant

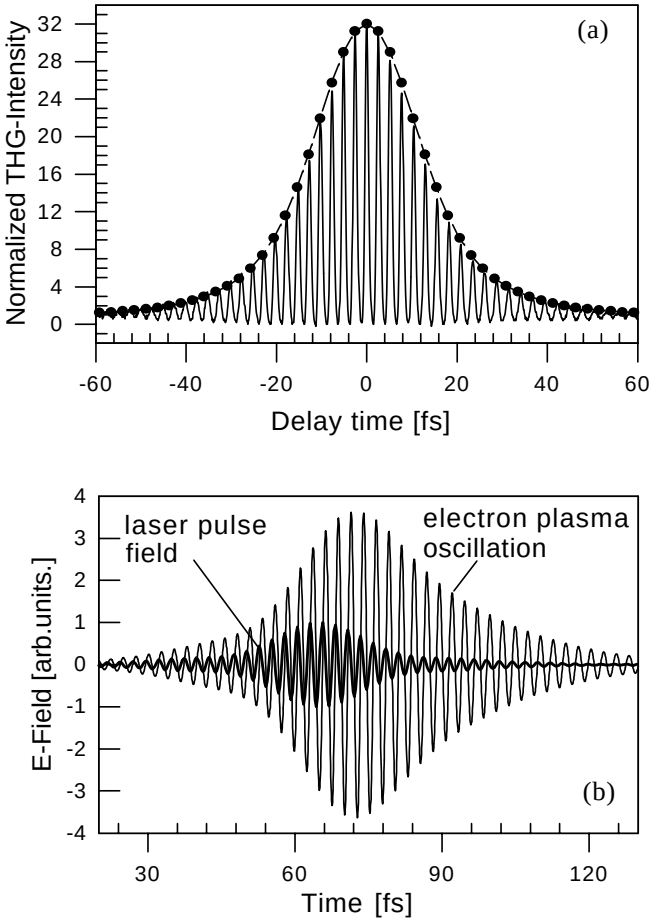

FIG. 2. (a) Solid line: measured third order ACF for a *resonantly* excited particle plasmon (extinction maximum of the nanoparticles at 774 nm), maximum normalized to 32; filled circles: envelope of the calculated ACF (the dashed line serves as a guide to the eye). (b) Driving laser pulse field together with the calculated *resonant* plasmon field oscillation ($\lambda_{\text{res}} = 774$ nm, $\tau = 6$ fs).

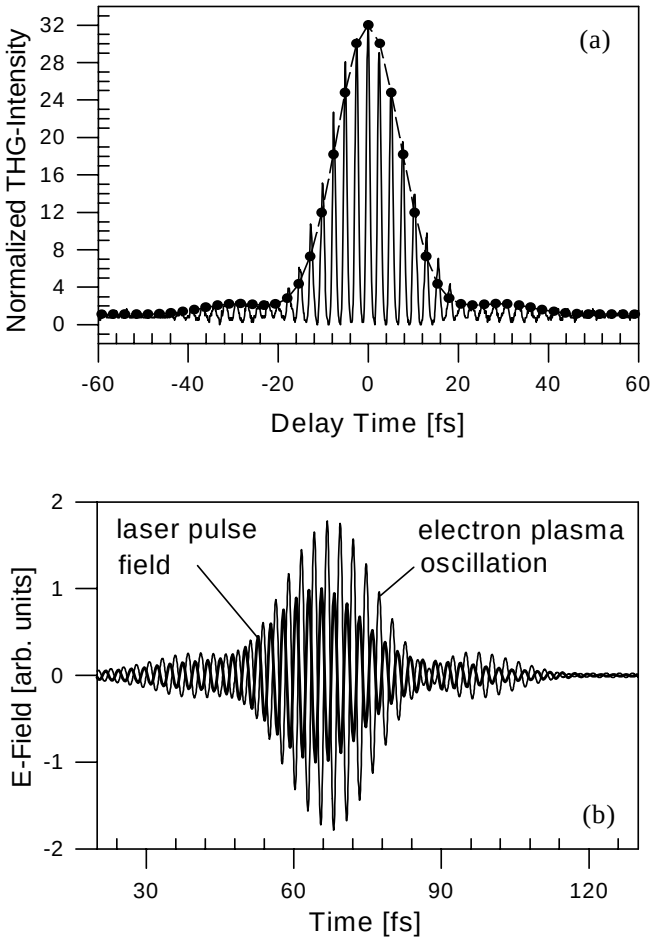

FIG. 3. (a) Solid line: measured third order ACF for an *off resonantly* excited particle plasmon (extinction maximum of the nanoparticles at 860 nm), maximum normalized to 32; filled circles: envelope of the calculated ACF (the dashed line serves as a guide to the eye). (b) Driving laser pulse field together with the calculated *off-resonant* plasmon field oscillation ($\lambda_{\text{res}} = 860$ nm, $\tau = 6$ fs).

case (Fig. 3b) shows that the phase difference between the driving laser field and the driven plasmon oscillation is no longer constant at $\pi/2$ as in the resonant case (Fig. 2b), but varies with time (beating). As seen in Fig. 3b the plasmon oscillation amplitude is strongly decreased when the phase difference approaches π, an effect that gives rise to the observed side wings in the ACF and the reduced FWHM, respectively. The beating between driving laser field and the particle plasmon oscillation in the off-resonant case demonstrates clearly the nature of the plasmon as a collective coherent oscillation of the plasma electrons.

Besides the different time characteristics of resonantly and off resonantly driven particle plasmons we also find different plasmon oscillation amplitudes; see the scales in Figs. 2b and 3b, respectively. We examine this effect in detail by measuring the relative values of the THG intensities of resonant and *off*-resonant driven particle plasmons. As in this case we need no time resolution; no sweep of the time delay in the autocorrelator is applied, i.e., $t' = 0$. THG intensities measured with the laser pulse shown in Fig. 1c are marked as filled circles in Fig. 4 as a function of the resonance frequency of the respective nanoparticle samples. The THG intensity values are normalized to the THG intensity obtained by the ITO coated quartz substrate. For particles with resonance frequencies below 700 nm or beyond 860 nm this normalization becomes meaningless as the particles deliver less THG intensity than the substrate itself. Therefore an absolute determination of the resonance induced THG enhancement factor is not feasible. Furthermore the measured THG intensities have to be corrected with respect to absorption of the driving laser field as the different samples consist of particles with different volumes and thus different absorption cross sections. A constant particle volume could not be maintained in our experiments due to the tuning of the resonance frequency by varying the particle diameter. The THG values corrected for constant absorption are shown by the open circles in Fig. 4. For comparison with theory we now calculate the THG intensity as a function of the resonance frequency in the spectral range between 710 and 860 nm. For excitation we assume the laser pulse

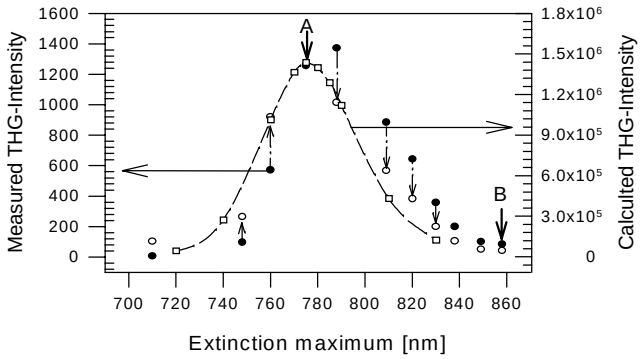

FIG. 4. Filled circles: measured THG intensities as a function of the resonance frequencies of the respective nanoparticle samples (normalized to the THG intensity obtained by the ITO coated quartz substrate). Open circles: measured THG intensities corrected for constant laser pulse absorption. Squares: calculated THG intensities (the dashed line serves as a guide to the eye). The letters *A* and *B* mark the THG intensities of the resonantly and off resonantly driven particle plasmons shown in Figs. 2 and 3, respectively.

field obtained above (Fig. 1c). We end up with the following expression for the THG intensity $I^{(3\omega)}$:

$$I^{(3\omega)} \propto \int |E_{\mathrm{Pl}}(t)|^6 \, dt \,. \tag{2}$$

For this calculation we assume $\tau = \text{const} = 6$ fs for the spectral range considered. This approximation is reasonable considering the damping mechanisms (Landau and radiation damping [1]) in the spectral range under investigation. The result of the calculation is plotted by the squares in Fig. 4. In the calculation we are not limited by any substrate THG contributions. We used an experimentally unrealistic large wavelength ($\lambda_{\mathrm{res}} = 10$ μm) to ensure a *nonresonant* THG value to be taken as reference for the normalization of the calculated THG values. The qualitative agreement between measured and calculated spectral characteristic of the THG intensity is quite good, especially in the spectral region near the laser center wavelength. As mentioned above, quantitative agreement cannot be achieved due to THG generation of the substrate. Relying on the calculated maximum THG intensity of 1.4×10^6 we deduce a resonance induced plasmon field enhancement of $\sqrt[6]{1.4 \times 10^6} \approx 11$. Note that this enhancement factor is valid only for the excitation with the fs pulses used in our experiment (nonstationary case). For the stationary case the amplitude enhancement factor is found by the stationary harmonic oscillator model (resonance frequency 774 nm, $\tau = 6$ fs) to be equal to 14. This factor should not be mixed up with the conventionally used term "field enhancement," which describes the enhancement of the optical near field compared to the incoming field. This field enhancement around a nanoparticle is strongly dependent on the considered position on the particle surface. In our case the factor of 11 means that the surface averaged plasmon field strength for a resonantly driven particle plasmon is 11 times larger than for the nonresonant driven plasmon.

In summary, we have shown that measuring the THG-ACF is a suitable method for evaluating the time characteristics of fs driven plasmon oscillations in metal nanoparticles. Resonant and off-resonant excitation of particle plasmons can be clearly distinguished by the ACF measurements. The excellent agreement of the measured ACFs with our calculations shows that the light-driven damped harmonic oscillator is a suitable model for plasmon oscillations in a metal nanoparticle. In particular, in the off-resonant case the beating between the driving field and the plasmon field demonstrates the nature of the plasmon oscillation as a collective electron oscillation. In contrast to previous ACF measurements based on SHG, THG experiments can also be performed using centrosymmetrically shaped particles, a fact which increases the practicability of this method. The electron-beam-lithographic method for sample preparation allows an exact tuning of the resonance frequencies of the particle plasmons. Plasmon resonance as a source of enhanced optical nonlinearity together with a fs time scale response time are features which could make metal nanoparticles promising nonlinear devices in a future submicron light technology (nano-optics).

Financial support by the Austrian Federal Ministry for Science and Traffic, Technology Division, and by the European Union (TMR Project NanoSNOM) is gratefully acknowledged.

[1] U. Kreibig and M. Vollmer, *Optical Properties of Metal Clusters*, Springer Series in Material Science Vol. 25 (Springer, Berlin, 1995).
[2] B. Lamprecht, A. Leitner, and F. R. Aussenegg, Appl. Phys. B **64**, 269 (1997).
[3] J.-H. Klein-Wiele, P. Simon, and H.-G. Rubahn, Phys. Rev. Lett. **80**, 45 (1998).
[4] M. Simon, F. Träger, A. Assion, B. Lang, S. Voll, and G. Gerber, Chem. Phys. Lett. **296**, 579 (1998).
[5] B. Lamprecht, A. Leitner, and F. R. Aussenegg, Appl. Phys. B **68**, 419 (1999).
[6] W. Gotschy, K. Vonmetz, A. Leitner, and F. R. Aussenegg, Opt. Lett. **21**, 1099 (1996); W. Gotschy, K. Vonmetz, A. Leitner, and F. R. Aussenegg, Appl. Phys. B **63**, 381 (1996).
[7] H. Voltz, *Einführung in die theoretische Mechanik I* (Akademische Verlagsgemeinschaft, Frankfurt, 1971).
[8] D. Meshulach, Y. Barad, and Y. Silberberg, J. Opt. Soc. Am. B **14**, 2122 (1997).
[9] J.-C. M. Diels, J. J. Fontaine, I. C. McMichael, and F. Simoni, Appl. Opt. **24**, 1270 (1985).
[10] A. Stingl, Ch. Spielmann, F. Krausz, and R. Szipcs, Opt. Lett. **19**, 204 (1994).
[11] Ch. Spielmann, L. Xu, and F. Krausz, Appl. Opt. **36**, 2523 (1997).
[12] B. Lamprecht, A. Leitner, and F. R. Aussenegg, Appl. Phys. B **69**, 223 (1999).
[13] H. B. Liao *et al.*, Opt. Lett. **23**, 388 (1998).
[14] C. Flytzanis *et al.*, Prog. Opt. **XXIX**, 321 (1991).